Journal of Applied Physics

Thermoelastic modeling of laser-induced generation of strong surface acoustic waves

Cite as: J. Appl. Phys. **130**, 185108 (2021); https://doi.org/10.1063/5.0071170
Submitted: 12 September 2021 • Accepted: 21 October 2021 • Published Online: 11 November 2021

Maxim V. Shugaev and Leonid V. Zhigilei

AIP Publishing

Journal of Applied Physics ARTICLE scitation.org/journal/jap

Thermoelastic modeling of laser-induced generation of strong surface acoustic waves

Cite as: J. Appl. Phys. **130**, 185108 (2021); doi: 10.1063/5.0071170
Submitted: 12 September 2021 · Accepted: 21 October 2021 ·
Published Online: 11 November 2021

Maxim V. Shugaev and Leonid V. Zhigilei[a)]

AFFILIATIONS

Department of Materials Science and Engineering, University of Virginia, 395 McCormick Road, Charlottesville, Virginia 22904-4745, USA

[a)]**Author to whom correspondence should be addressed:** lz2n@virginia.edu

ABSTRACT

Short pulse laser irradiation of a substrate can generate pulses of surface acoustic waves (SAWs) capable of propagating long distances along the surface of the irradiated substrate. In this work, we use thermoelastic modeling of the generation of SAWs on a Si substrate to explore the effect of irradiation parameters, i.e., pulse duration, laser spot size, absorption depth, and spatial profile of the laser energy deposition, on the strength of the SAWs. A particular goal of this study is to establish the optimum conditions for maximizing the strength of the surface waves generated in the nonablative, thermoelastic irradiation regime. The simulations demonstrate that the highest strain amplitude of the laser-generated SAWs can be achieved for a laser spot size comparable to the characteristic length of the SAW propagation during the laser pulse. The amplitude of SAWs increases with the increase in the characteristic laser energy deposition depth, and laser pulses with sharper spatial energy deposition profiles (flat-top laser beams) produce stronger SAWs. For the optimal set of irradiation parameters, the strain amplitude of a SAW generated in Si in the thermoelastic regime can reach the levels of 10^{-4}–10^{-3}, which are sufficiently high for causing nonlinear sharpening of the wave profile and the formation of a shock front during the wave propagation from the laser spot. The computational predictions suggest the feasibility of a continuous generation of strong nonlinear pulses of SAWs, which may be utilized for driving the surface processes in thin film deposition, growth of two-dimensional materials, heterogeneous catalysis, and other applications.

I. INTRODUCTION

The generation of acoustic waves in solids by short pulse laser irradiation is at the basis of a number of practical applications, particularly in the area of nondestructive evaluation of material properties[1,2] and the detection of heterogeneities and crystal defects.[3–5] Moreover, there is emerging evidence that the acoustic waves can be used not only for probing the material structure and properties, but also for material modification and the acoustic activation of atomic- or molecular-level surface processes.[6] In particular, the ability of strong photoacoustic pulses to cause the desorption/ejection of atoms, molecules, and thin molecular overlayers from the surface has enabled the development of Laser-Induced Acoustic Desorption (LIAD) mass spectrometry technique.[7–13] The ejection of submicrometer nanoparticles driven by laser-generated surface acoustic waves (SAWs) has been suggested as an effective surface cleaning approach suitable for integration into microcircuit manufacturing technologies.[14,15] Strong laser-generated SAWs have also been observed to produce quasi-periodic arrays of cracks in brittle materials, such as Si[16–18] and fused silica,[18] to facilitate crystallization in amorphous MoS_2 films,[19] and to produce a large enhancement of surface diffusion of Au clusters on a Si substrate.[20,21]

The ability of an acoustic wave to cause the material or surface modification often relies on the sharpening of the wave profile and eventual shock front formation during the wave propagation in a material exhibiting nonlinear elastic properties.[22,23] In particular, a recent computational study of acoustic desorption has identified the resonant coupling of high-frequency harmonics of the nonlinear bulk acoustic waves with the vibrational modes of the surface adsorbates and thin overlayers as the key process responsible for the desorption of atomic clusters and exfoliation if thin graphene multilayers.[24] A similar mechanism based on the nonlinear sharpening of laser-generated SAWs has been suggested[21] as an explanation of the experimentally observed acoustic enhancement of surface diffusion of atomic clusters.[20,21] The nonlinear transformation of the SAW pulses has also been observed to increase the surface acceleration and to facilitate the acoustic cleaning process.[14]

Moreover, for a sufficiently strong laser-generated SAW, the nonlinear sharpening and cusping of the wave profile[25,26] can lead to a gradual increase in the surface strain above the initial strain amplitude of the wave, up to the levels high enough for the generation of subsurface defects[27] or the onset of surface cracking at some distance from the wave source.[16–18]

The formation of a shock front and, more generally, the extent of nonlinear sharpening of the wave profile are defined by the nonlinearity of the elastic properties of the substrate material, the initial wave amplitude, and the distance traveled by the wave through the substrate. The shock front formation distance for an initially harmonic (sinusoidal) wave is commonly described[27,28] as $L_{sh} = 1/(\beta e_0 k)$, where β is the effective nonlinearity parameter of the material, e_0 is the initial surface strain amplitude, $k = 2\pi/\lambda$ is the spatial angular frequency (wavenumber), and λ is the wavelength. For SAWs, the nonlinearity parameter β is usually on the order of unity,[27–29] the minimum wavelength of a wave generated by a short laser pulse is on the order of 100 μm (about twice the size of the laser spot),[2] and the wave amplitude e_0 required for the generation of the shock front at 1–100 mm from the source can be estimated to range from 10^{-2} to 10^{-4}. Note that a weaker acoustic wave may never develop the shock front, since the frequency-dependent dissipation of the higher-order harmonics[25–27] may balance the nonlinear frequency up-conversion and suppress the sharpening of the wave profile.

The strong SAWs with strain amplitudes up to 10^{-2} can be readily produced by direct laser ablation of the substrate or by using a sacrificial ablating layer, such as a liquid suspension of carbon particles.[14,16–18] The ablative generation of SAWs, however, limits the number of laser pulses that can be applied for the reliable generation of SAWs[30] and can produce undesirable surface contamination by ablation debris. The generation of the SAWs in the nonablative irradiation regime has obvious advantages, particularly for applications that rely on continuous utilization of acoustic energy. One example of such applications is the acoustic activation of surface diffusion,[20,21,31,32] proposed as a possible solution to a challenging problem of thin film growth on heat-sensitive substrates.[21,31] Since the mechanism of the diffusion enhancement suggested by the results of atomistic simulations[21] is relying on the nonlinear sharpening of SAWs, it is important to confirm that the amplitudes of SAWs generated in the experimental studies of the diffusion enhancement[20,21] are sufficiently high for inducing the nonlinear sharpening of the waves at a distance of about 10 mm from the laser spot. While the common notion is that SAWs generated in the nonablative regime are usually too weak for exhibiting a pronounced nonlinear behavior,[2,29] the estimations of the maximum normal surface displacement produced by a SAW generated in an aluminum substrate in the thermoelastic regime[1] suggest that the strain amplitude of the wave can approach $\sim 10^{-3}$ with an appropriate choice of the width of the laser beam.

In this article, we report the results of a systematic computational analysis of the ability of short pulse laser irradiation to generate SAWs with strain amplitudes that are sufficiently high for causing nonlinear sharpening and shock front formation during the wave propagation along the surface of the substrate. The conditions of the experiments on the acoustic activation of surface diffusion[20,21] are considered first, and the feasibility of the generation of strong nonlinear SAWs in these experiments is confirmed. The investigation is then extended to the analysis of the effect of irradiation parameters, such as pulse duration, laser spot size, absorption depth, and the shape of the laser beam profile, with the goal of identifying the conditions that maximize the efficiency of the SAW generation in the nonablative irradiation regime.

II. COMPUTATIONAL MODEL

The computational description of the laser-induced generation of stress waves and the dynamic evolution of thermoelastic stresses is provided in this work in the framework of the thermoelasticity model that combines the thermal model based on the heat diffusion equation with the thermoelastic wave equation,[33–38]

$$c_p \rho \frac{\partial T}{\partial t} = \nabla k_{\text{th}} \nabla T + S - \alpha_L T C_{iimn} \frac{\partial^2 u_m}{\partial t \partial x_n}, \tag{1}$$

$$\rho \frac{\partial^2 u_i}{\partial t^2} = \frac{\partial \sigma_{ij}}{\partial x_j} = C_{ijmn} \left[\frac{\partial^2 u_m}{\partial x_j \partial x_n} - \delta_{mn} \alpha_L \frac{\partial T}{\partial x_j} \right], \tag{2}$$

$$\sigma_{ij} = C_{ijmn} \left[\frac{\partial u_m}{\partial x_n} - \delta_{mn} \alpha_L (T - T_0) \right], \tag{3}$$

where T, c_p, ρ, k_{th}, u_i, σ_{ij}, α_L, and C_{ijmn} are temperature, heat capacity, density, thermal conductivity, displacement, stress tensor, linear thermal expansion coefficient, and stiffness tensor, respectively. The source term S describes the laser energy deposition as explained below. The transient heating/cooling induced by adiabatic compression/expansion of the material during wave propagation is accounted for by a term $-\alpha_L T C_{iimn} \frac{\partial^2 u_m}{\partial t \partial x_n}$ in Eq. (1), although the effect of this term on the temperature distribution is negligible for the irradiation conditions considered in the present study (the temperature variation due to this term does not exceed 1 K for the wave amplitudes below 10^{-3}). Since the simulations are performed for a highly anisotropic material, single crystal silicon, the general expression of the stress tensor is used in Eqs. (1)–(3) in lieu of a commonly used formulation for isotropic materials.[34,35]

The simulations are performed for a computational setup illustrated in Fig. 1. The equations are formulated for the two-dimensional (2D) Cartesian coordinate system, with a uniform temperature and zero strain assumed along the third direction. This setup is motivated by the common use of rectangular laser spots (the length of the laser spot in one direction is much longer than in another one) in experimental studies where straight-crested SAWs are produced by focusing laser pulses by cylindrical lenses.[2,16–21,26,30,39,40] The source term S in Eq. (1) reproduces a Gaussian temporal profile of the laser pulse and an attenuation of the deposited laser energy with depth, along the y axis, described by the Beer–Lambert law. To investigate the effect of the spatial energy deposition, the simulations were performed with either Gaussian or flat-top spatial laser beam profiles.

Since Si substrates are used in many experimental studies of laser-induced SAWs,[16–18,20,21,30,39,40] the simulations are performed for a single crystal Si (100) substrate described by the following parameters: elastic moduli $C_{11} = 165.78$ GPa, $C_{12} = 63.94$ GPa,

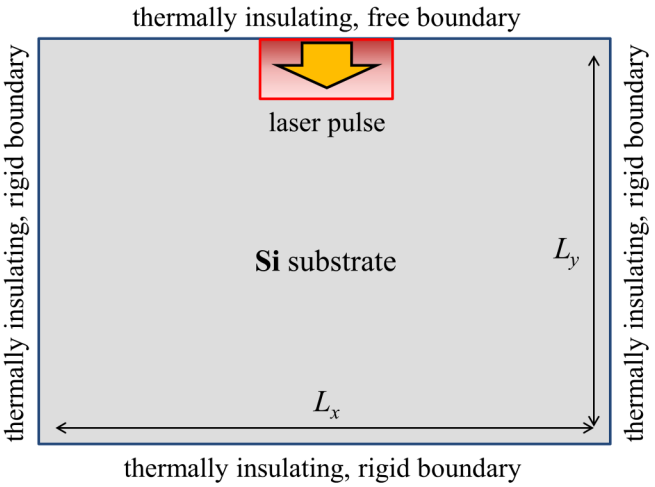

FIG. 1. Schematic illustration of the computational system used in 2D thermoelastic modeling of laser irradiation of a Si substrate.

$C_{44} = 79.62$ GPa, density $\rho = 2328\,\mathrm{kg/m^3}$, heat capacity $c_p = 702\,\mathrm{J\,kg^{-1}\,K^{-1}}$, thermal conductivity $k_{\mathrm{th}} = 124\ \mathrm{Wm^{-1}\,K^{-1}}$, and linear thermal expansion coefficient $\alpha_L = 2.49 \times 10^{-6}\,\mathrm{K^{-1}}$.[41] With the elastic moduli listed above, the speed of SAWs on the (100) Si substrate along the [001] direction is found to be 4920 m/s through an analytical solution to the elasticity equation for the Si substrate with a free surface.[27,42] This velocity is close to the ones measured experimentally[43,44] and derived analytically[44] for the same system.

The use of the constant room-temperature material parameters and the linear nature of Eqs. (1)–(3) [except for the last term in Eq. (1), which, as noted above, has a negligible contribution to the generation and evolution of SAWs] makes it possible to directly map the results of the simulations obtained at a given laser fluence to other fluences in the thermoelastic regime by linearly scaling the values of strain with the laser fluence. Meanwhile, the temperature dependences of the heat capacity (c_p increases to 1030 $\mathrm{J\,kg^{-1}\,K^{-1}}$ at $T = T_m = 1687$ K)[45] and the thermal expansion coefficient (α_L increases to $4.56 \times 10^{-6}\,\mathrm{K^{-1}}$ at $T = 1500$ K)[46] have opposite effects on the strength of the laser-generated SAWs and can be expected to partially compensate each other.

For the heat transfer equation, thermally insulating boundary conditions are applied in all four directions. For the displacements, rigid boundary conditions are applied at the bottom, left, and right sides of the system, while free boundary condition is imposed at the top surface. The system size is selected so that the stress waves do not reach the rigid boundaries during the time of the simulations. The number of cells is 10 000 in the x-direction, and 5000–6000 cells in the y-direction, depending on conditions considered in the simulations. The spatial resolution of the mesh is defined based on the size of the laser spot to ensure an accurate description of the acoustic wave generation.

The equations for the displacement, Eq. (2), are solved using an explicit Euler method, with the timestep of integration set based on a condition of $\theta = C_{11}\Delta t^2/\rho\Delta x^2 = 0.6$. While implicit schemes are not limited by a condition of $\theta \leq 0.6$, they introduce strong numerical dispersion and require special consideration in 2D and 3D simulations. For the thermal part, Eq. (1) is solved with explicit Euler or Alternating Direction Implicit (ADI) algorithms, with the former imposing the condition of $\zeta = k_{\mathrm{th}}\Delta t/c_p\rho\Delta x^2 < 0.25$. The ADI algorithm, applied when $\zeta \geq 0.25$, is slightly slower than the explicit Euler but enables simulations with $\zeta = 25 - 50$, which shortens the overall time of the simulation. The free boundary condition is implemented in an implicit formulation suggested in Ref. 47, which provides a stable solution in the whole range of simulation parameters used in the present study.

III. RESULTS AND DISCUSSION

In the first application of the model described in Sec. II, we consider the generation of SAWs under conditions similar to those of an experimental study of the acoustic activation of surface diffusion.[21] Specifically, a Si substrate is irradiated at a wavelength of 355 nm by a laser pulse with a duration of $\tau_L = 6$ ns, where τ_L is defined as the full width at half-maximum (FWHM) of the Gaussian temporal profile. To ensure complete deposition of the laser pulse energy to the target, the maximum of the Gaussian temporal profile is shifted with respect to the start of the simulation (zero time) by 2.5 τ_L, i.e., the peak intensity of the laser pulse corresponds to a time of 15 ns.

The width of the laser beam in the x-direction (defined as FWHM of the Gaussian spatial profile and denoted as d) is 16 μm, which is close to the width of a rectangular laser spot produced by a cylindrical lens in the experiments.[21] The FWHM definition of the spot size is used here in lieu of a more common $1/e^2$ definition to facilitate the comparison of the results obtained with the Gaussian and flat-top laser beam profiles. As revealed in the simulations discussed below, the characteristic width of the laser energy deposition has a substantial effect on the amplitude of the laser-generated SAWs. With the $1/e^2$ definition of the Gaussian laser spot width, the energy deposition profile is much narrower, and the maximum laser fluence at the center of the laser spot is much higher (by ~60% for a rectangular spot) as compared to the flat-top laser beam of the same nominal width and the same laser pulse energy. The FWHM definition of the spot size, on the other hand, yields an energy deposition profile comparable to that of the flat-top laser beam and the maximum laser fluence at the center of the laser spot that is only 6% less than the fluence of the flat-top pulse of the same width and energy. As a result, the physical interpretation of the computational predictions is more straightforward when the FWHM definition of the Gaussian laser spot width is used. The much longer 5 mm length of the experimental rectangular laser spot in the direction perpendicular to the plane of the plot in Fig. 1 justifies the 2D representation of the system in the simulations. The total system size, $L_x \times L_y$, is $2 \times 1.2\ \mathrm{mm^2}$, the spatial resolution of the mesh is 0.2 μm, and the time step is about 18.4 ps.

The characteristic depth of material heating during the laser pulse, λ_{dep}, is defined by the optical penetration depth or the depth of the thermal energy redistribution by the heat diffusion into the target, whichever is larger. For irradiation at a wavelength of 355 nm, the optical absorption depth is only 9 nm, and λ_{dep} is

largely defined by heat diffusion during the laser pulse, i.e., $\lambda_{dep} \approx \sqrt{2D_{th}\tau_L} \approx 0.9\,\mu$m, where $D_{th} = k_{th}/(\rho c_p) \approx 7.5910^{-5}$ m^2/s is thermal diffusivity. The experimental incident laser fluence of 0.75 J/cm^2 is converted to the absorbed fluence of 0.315 J/cm^2 using the reflectivity of 0.58 at a wavelength of 355 nm.[48] The absorbed fluence used in the simulations is further reduced to 0.25 J/cm^2 to bring the maximum temperature reached in the substrate to 1650 K, just below the melting temperature of silicon, $T_m = 1687$ K.[41]

This reduction of laser fluence can be justified as follows. According to the calculations performed with the model described in Sec. II, the maximum temperature reaches ~2000 K at the experimental absorbed fluence of 0.315 J/cm^2 (assuming Gaussian spatial beam profile with width defined as FWHM). These calculations, however, do not account for the melting process, and, given the large heat of melting of Si, $\Delta H_m = 50$ kJ/mol,[45] the melting depth can be expected to be very shallow under the experimental conditions. Indeed, with $C_p(T_m) = 29$ J/(mol K),[45] one can estimate the temperature variation equivalent to the complete melting of Si as $\Delta T = \Delta H_m/C_p(T_m) = 1724$ K, which is more than 5 times larger than the level of superheating above T_m predicted in the simulations. Moreover, the onset of melting in Si has been observed to result in the saturation and even a small decrease in the amplitude of SAWs generated by nanosecond pulse irradiation of Si substrates.[30,40] These observations have been explained by the negative volume of melting of Si, the loss of shear rigidity upon melting that diminishes the contribution of the molten layer to the generation of SAWs, and the decrease in the heat flux into the solid part of the substrate due to the partial transformation of the deposited laser energy into the heat of melting.[40] Further increase in the laser fluence leads to a sharp increase in the amplitude and changes in the shape of the laser-generated SAW pulse at the onset of the collective material ejection (ablation) triggered by the explosive boiling of Si[49] heated to the levels comparable to the critical temperature, $T_c = 5159$ K.[50] Since the experimental conditions of Ref. 21 are substantially below the ablation threshold, the scale down of the fluence to just below the melting threshold should provide a reliable order of magnitude estimate of the SAW amplitude while avoiding the complications and uncertainty related to the introduction of the description of melting into the thermoelastic model.

The simulation of the laser-induced generation of the acoustic waves is performed for a time sufficiently long for the formation of well-defined SAWs propagating away from the laser spot but shorter than the time needed for the waves to reach the boundaries of the computational system. A snapshot from the simulation taken at a time of 100 ns and illustrating the distribution of the density of thermoelastic energy is shown in Fig. 2. The energy density includes the contributions from the longitudinal and shear bulk waves, SAWs, and quasistatic stresses in the vicinity of the laser spot related to the temperature gradients. It does not include the

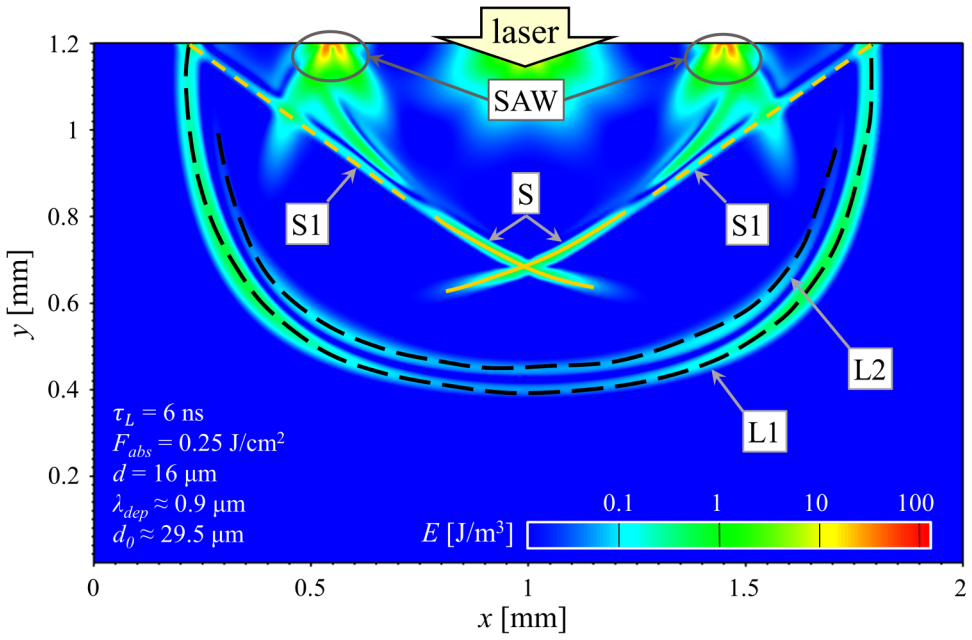

FIG. 2. The distribution of the thermoelastic energy density at a time of 100 ns predicted in a simulation of a silicon substrate irradiated by a 6 ns laser pulse at a wavelength of 355 nm and an absorbed fluence of 0.25 J/cm^2. The irradiation conditions are comparable to those used in the experiments described in Ref. 21. The laser beam has a Gaussian spatial profile along the x axis with a width d of 16 μm, the characteristic depth of the laser energy deposition/redistribution during the laser pulse, λ_{dep}, is about 0.9 μm, and the characteristic length of the SAW propagation during the laser pulse, d_0, is about 29.5 μm. The laser-induced longitudinal and shear bulk waves are schematically marked by black and yellow lines, respectively. The labels denote the surface acoustic waves (SAW), the compressive (L1) and tensile (L2) components of the longitudinal wave, the shear waves generated by the rapid laser heating (S), and the interaction of the longitudinal wave with the free surface of the substrate (S1). The quasistatic thermal stresses related to the temperature gradients produced by laser energy deposition are also present in the vicinity of the laser spot.

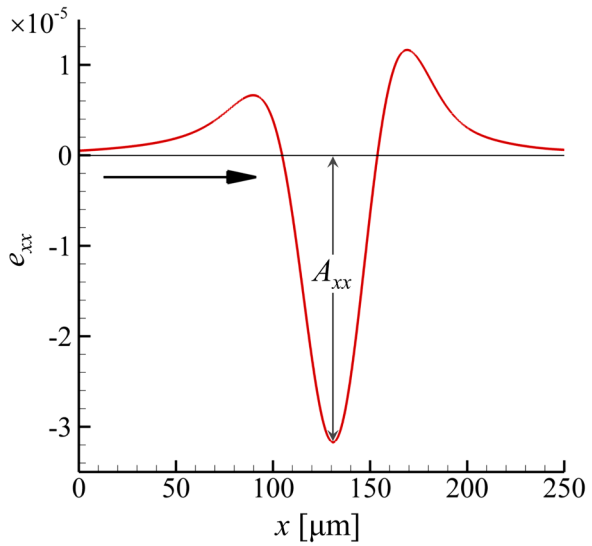

FIG. 3. The profile of surface strain e_{xx} of a laser-generated SAW pulse predicted in a simulation performed at $\tau_L = 6$ ns, $F_{abs} = 0.25$ J/cm^2, $d = 32$ μm, and a flat-top laser beam profile. These conditions correspond to $\lambda_{dep} \approx 0.9$ μm and $d_0 \approx 29.5$ μm. The horizontal arrow shows the direction of the SAW pulse propagation. The strength of the SAW pulse is characterized by the amplitude A_{xx} marked on the plot.

contribution of the thermal energy deposited by the laser pulse. Although the laser irradiation leads to the generation of a variety of waves propagating into the bulk of the substrate, the focus of the present study is on the two broadband SAW pulses launched from the laser spot and propagating in the opposite directions along the surface of the substrate. The strain produced by the SAW pulses ranges from -2.45×10^{-5} to 0.95×10^{-5} for e_{xx} and from -0.75×10^{-5} to 1.0×10^{-5} for e_{yy} components. The maximum level of strain is reached at the surface of the substrate for e_{xx} and at some depth under the surface for e_{yy}.

To check the effect of the shape of the spatial profile of the laser beam on the SAW generation, we have performed an additional simulation under the same conditions as the simulation discussed above but with a flat-top laser energy distribution profile along the x axis instead of the Gaussian one. With the flat-top laser beam, the amplitude A_{xx} of the SAW pulse is found to increase by about 16%, from 2.45×10^{-5} to 2.85×10^{-5}. This observation suggests that the sharpness of the spatial profile of the laser energy deposition may lead to a moderate increase in the efficiency of the SAW generation. A typical profile of surface strain e_{xx} obtained in the simulation of laser generation of SAW pulses is shown in Fig. 3 for the conditions similar to those used in the simulation illustrated in Fig. 2, but for a twice larger width of the laser beam, $d = 32$ μm, and the flat-top laser beam. These conditions are close to the optimal ones for the generation of strongest SAW pulses by 6 ns pulses at a wavelength of 355 nm.

Since Eqs. (1)–(3) do not account for the nonlinearity of elastic properties of the material, the SAW pulse propagates without sharpening of the wave profile and formation of a shock front in the simulations. The SAW amplitude $A_{xx} = 2.45 \times 10^{-5}$ predicted for the experimental conditions of Ref. 21 or $A_{xx} = 3.17 \times 10^{-5}$ predicted for a twice wider flat-top laser beam (Fig. 3), however, may be sufficiently high to expect a substantial nonlinear distortion of the SAW pulse profile during the pulse propagation in a real Si substrate exhibiting a pronounced nonlinear behavior.[16–18,30] Moreover, it has been noted[51] that the nonlinear evolution of a broadband laser-generated SAW pulse can be expected to be more pronounced than that of a sinusoidal wave, as the nonlinear frequency up-conversion occurs in a large spectral range. Nevertheless, a further increase in the strength of the SAW pulses generated in the thermoelastic regime would benefit the applications. Thus, the optimization of the irradiation conditions focused on increasing the strength of the SAW pulses is discussed next.

The dependence of the wave amplitude and energy on the size of the laser spot is explored next in a series of simulations where the width of the flat-top laser beam d was varied from 0.5 to 256 μm, while all other irradiation parameters are kept the same as in the simulations discussed above. The results of the simulations are shown in Fig. 4, and the interpretation of the results can be

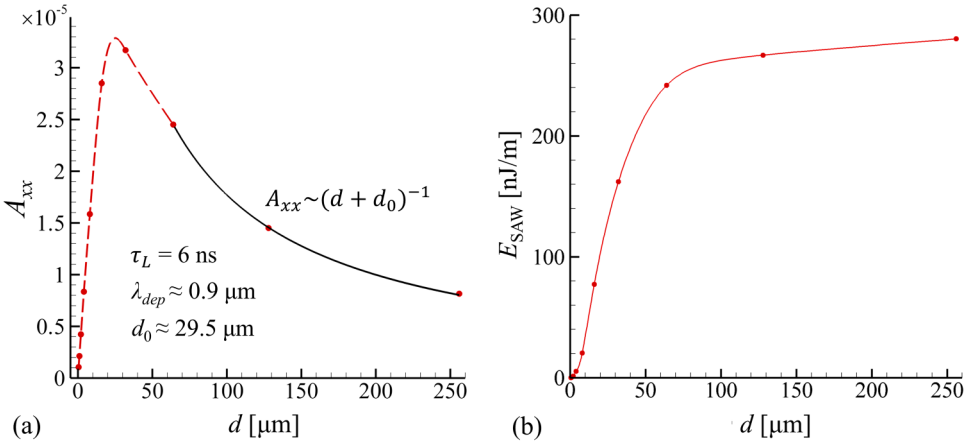

FIG. 4. The laser spot size dependence (flat-top laser beam profile) of the amplitude (a) and the energy per unit length of the wave front (b) of a SAW pulse generated in simulations of laser irradiation of a Si substrate. The laser pulse duration of $\tau_L = 6$ ns corresponds to the thermal diffusion length $\lambda_{dep} \approx 0.9$ μm and wave propagation distance of $d_0 \approx 29.5$ μm during the laser pulse. The black solid line in (a) shows the result of fitting the scaling law $A_{xx} \sim (d + d_0)^{-1}$ to the three data points with $d \geq 64$ nm.

guided by the conclusions of an analytical study of elastic waves emitted from circular elements vibrating normally to the surface of a semi-infinite substrate.[52] According to this study, the scaling of energy of a SAW emitted from a circular laser spot with the spot diameter d depends on whether the spot diameter is smaller or larger than the characteristic length of the SAW propagation during the time of laser irradiation, $d_0 = \tau_L v_{SAW}$. The energy scales as $E_{SAW} \sim d^2$ for $d \ll d_0$ and as $E_{SAW} \sim d$ for $d \gg d_0$. A similar analysis based on the consideration of a rectangular laser spot as a linear arrangement of point sources gives $E_{SAW} \sim d^2$ for $d \ll d_0$ and $E_{SAW} \sim$ const for $d \gg d_0$. At distances smaller than the SAW wavelength λ, the interference of a set of coherent point sources leads to a square increase of the total energy, while a destructive interference of sources separated by a distance comparable to (or larger than) λ gives a constant value. For $d \ll d_0$, the SAW wavelength λ is mostly dictated by the pulse duration and does not depend on the spot diameter. Meanwhile, for $d \gg d_0$, the SAW wavelength increases proportionally to the spot size, i.e., $\lambda \sim d + d_0$. Since the energy localization near the surface is proportional to λ for SAWs, $E_{SAW} \sim e_{xx}^2 \lambda^2$, and one can obtain the following scaling of the wave strain amplitude and energy on the spot size:

$$\begin{cases} A_{xx} \sim d, \quad E_{SAW} \sim d^2 & \text{for } d \ll d_0 \\ A_{xx} \sim (d + d_0)^{-1}, \quad E_{SAW} \sim \text{const} & \text{for } d \gg d_0. \end{cases} \tag{4}$$

These analytical scaling laws are in good agreement with the dependencies obtained in the simulations and depicted in Fig. 4. With $\tau_L = 6$ ns and $v_{SAW} = 4920$ m/s, the length of the SAW propagation during the laser pulse can be evaluated as $d_0 = \tau_L v_{SAW} \approx 29.5\,\mu$m. The wave amplitude A_{xx} exhibits a close-to-linear increase for $d \ll d_0$, reaches its maximum of about 3.17×10^{-5} at $d \approx d_0$, and decreases as $A_{xx} \sim (d + d_0)^{-1}$ upon further increase in d. The theoretical scaling and the computational predictions are also in agreement with the experimental data on the laser spot size dependence of the efficiency of the SAW generation in Al samples.[53]

To investigate the effect of pulse duration on the generation of SAWs, an additional series of simulations is performed for a pulse duration of 10 ps. Since the purpose of these simulations is to check how more than two orders of magnitude reduction of the pulse duration affects the generation of SAWs, we do not incorporate a detailed description of the kinetics of laser energy redistribution during the equilibration of the optically excited states in Si[54–56] into the model but simply assume the same Beer–Lambert laser energy deposition profile with the optical absorption depth of 9 nm as used in the simulations of nanosecond laser irradiation described above. The laser fluence is selected to be 0.01 J/cm^2, which gives approximately the same maximum temperature in the target as in the simulations performed with the longer 6 ns pulse. For small laser beam widths of $d < 250$ nm, the simulations are performed for systems with dimensions of $L_x \times L_y = 8 \times 4\,\mu$m^2, the spatial resolution of the mesh of 0.8 nm, and the time step of about 73.3 fs. To ensure that SAWs pass a sufficient distance from the irradiated area and the measured strain profiles are not affected by the static strain produced by the temperature increase in the region of laser energy deposition and by the laser-generated bulk waves, we increase L_x to

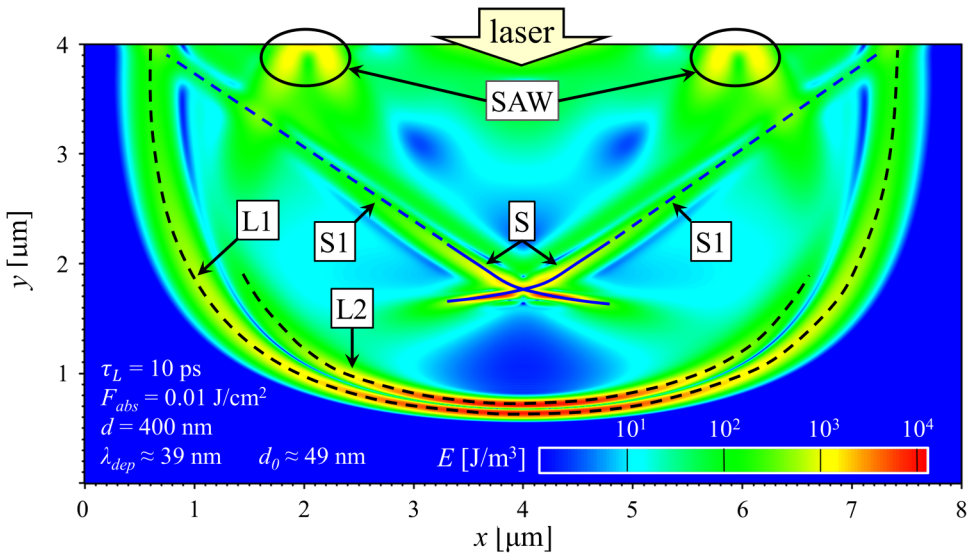

FIG. 5. The distribution of the thermoelastic energy density at a time of 403 ps predicted in a simulation of a silicon substrate irradiated by a 10 ps laser pulse at a wavelength of 355 nm and an absorbed fluence of 0.01 J/cm^2. The laser beam has a Gaussian spatial profile along the x axis with a width d of 400 nm, the characteristic depth of the laser energy deposition/redistribution during the laser pulse, λ_{th}, is about 39 nm, and the characteristic length of the SAW propagation during the laser pulse, d_0, is about 49 nm. The laser-induced longitudinal and shear bulk waves are schematically marked by black and blue lines, respectively. The labels denote the surface acoustic waves (SAW), the compressive (L1) and tensile (L2) components of the longitudinal wave, and the shear waves (S) generated by the laser energy deposition and the interaction of the longitudinal wave with the free surface of the substrate (S1). The quasistatic thermal stresses related to the temperature gradients produced by laser energy deposition are also present in the vicinity of the laser spot.

28 μm in simulations performed with wider laser spots, $d \geq 250$ nm.

A representative example of the distribution of thermoelastic energy density in a Si target irradiated by a 10 ps pulse with a width of the Gaussian spatial profile in the x-direction of 400 nm is shown in Fig. 5 for a time of 403 ps. The strain e_{xx} produced by the SAW pulses ranges from -1.45×10^{-4} to 4.25×10^{-5}. The generated acoustic pattern is qualitatively similar to the one shown in Fig. 2 for the longer laser pulse. The much more rapid energy deposition, however, creates the conditions close to the stress confinement,[49,57] when the heated material does not have time to fully expand in the vertical direction during the laser pulse, leading to the buildup of compressive stresses that, in turn, drive the emission of more intense longitudinal waves into the bulk of the substrate.

The fraction of the total energy deposited by the laser pulse that goes into the generation of the acoustic waves is about 1.1×10^{-4} in this simulation, and approximately 10% of the total acoustic energy is carried by SAWs. For comparison, in the simulation performed with 6 ns pulse and illustrated in Fig. 2, less than 10^{-5} of the deposited energy goes into the generation of the acoustic waves, but more than 70% of the acoustic energy corresponds to the SAWs.

Similar to the results obtained with longer 6 ns pulses, the irradiation by a 10 ps pulse with a flat-top laser beam profile along the x axis leads to the generation of stronger SAW pulses. In particular, for the simulation with $d = 400$ nm illustrated for the Gaussian beam profile in Fig. 5, the amplitude of the SAW pulses A_{xx} increases by more than a factor of two, from 1.45×10^{-4} to 3.8×10^{-4}, when the flat-top beam of the same width is applied.

The dependence of the amplitude and energy of a SAW pulse generated by a 10 ps laser pulse on the laser spot size is shown in Fig. 6. Similar to the longer 6 ns laser pulse irradiation considered above, the spot size dependence exhibits the two distinct regimes, a close-to-linear increase of A_{xx} for $d \ll d_0$ and $A_{xx} \sim (d + d_0)^{-1}$ decrease for $d \gg d_0$, with the strain amplitude going through the maximum at the transition between the two regimes. The maximum value of strain amplitude, 4.6×10^{-4}, is more than an order magnitude higher than that observed in the simulations performed with 6 ns pulse, Fig. 4, and the spot size corresponding to the maximum strain is shifted from $d \approx d_0$ in Fig. 4 to $d \approx 1.22 d_0$ in Fig. 6. Both the increase in the maximum strain amplitude and the shift of the optimal laser spot size to $d > d_0$ may be partially attributed to a depth of laser heating, $\lambda_{th} \approx 39$ nm, being comparable to the characteristic length of SAW propagation during the laser pulse, $d_0 \approx 49$ nm. As a result, the integral source cannot be considered as an infinitely thin plane of point sources, and the three-dimensional distribution of point sources must be accounted for. We note that the predicted optimal size of the laser spot for the generation of SAWs with the maximum amplitude is too small for practical applications. Even if the laser energy deposition is localized down to tens of nanometers, e.g., through the near-field enhancement techniques,[58–60] the energy of the produced SAW pulses [compare Figs. 4(b) and 6(b)] will still be too low for exhibiting any nonlinear effects during their long-range propagation. Indeed, since the laser spot size defines the wavelength λ of the SAW, the SAW energy is proportional to λ^2, and the active dissipation of the wave is localized at the shock front,[27] the rate of the wave decay during the nonlinear propagation increases with decreasing laser spot. Nevertheless, the results obtained for the short laser pulses suggest that the increase in the depth of the laser heating can substantially strengthen the laser-generated SAW pulses.

The effect of the laser energy deposition depth λ_{dep} on the characteristics of SAWs is investigated in an additional series of simulations performed with 6 ns laser pulse and a width of the spatial laser beam profile in the x-direction fixed at $d = 32$ μm, which is close to the optimum width for the generation of strong SAWs, as identified in the simulations discussed above. The laser fluence in each simulation is selected to ensure that the maximum temperature is the same as in the simulations discussed above, i.e., close but still below the melting temperature T_m. In contrast to the simulations performed for a fixed optical absorption depth of 9 nm, however, the optical absorption depth is used in the present series of simulations to control the laser energy deposition depth λ_{dep}. The absorption depth in Si exhibits a strong dependence on the laser wavelength and exceeds 1 and 100 μm as the wavelength increases above 510 and 980 nm, respectively.[48,61] In the present parametric study, we do not describe the results in terms of the

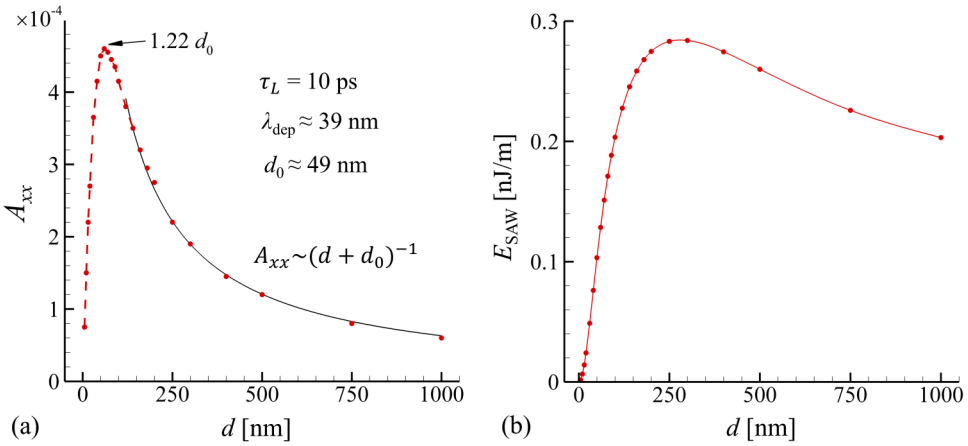

FIG. 6. The laser spot size dependence (Gaussian laser beam profile in the x-direction) on the amplitude (a) and the energy per unit length of the wave front (b) of a SAW pulse generated in simulations of laser irradiation of a Si substrate. The laser pulse duration of $\tau_L = 10$ ps corresponds to the thermal diffusion length $\lambda_{dep} \approx 39$ nm and wave propagation distance of $d_0 \approx 49$ nm during the laser pulse. The black solid line in (a) shows the result of fitting the scaling law $A_{xx} \sim (d + d_0)^{-1}$ to the data points with $d \geq 120$ nm.

laser wavelength but systematically change the absorption depth instead. To simplify the interpretation of the results, we neglect the contribution of the heat diffusion to the laser energy deposition depth and define λ_{dep} to be equal to the optical penetration depth, even though the heat diffusion does make a noticeable contribution to the temperature profile at the end of the laser pulse in the simulations performed with the shortest optical penetration depths of 1.3, 3.3, and 7.3 μm.

The dependence of the strain amplitude of the laser-generated SAW pulses on λ_{dep} is shown in Fig. 7. For a small depth of laser energy deposition relative to d_0, the energy of the generated SAWs is proportional to λ_{dep}^2, since the point sources located at different depths contribute coherently to wave generation. For the strain amplitude, this leads to $A_{xx} \approx \lambda_{dep}$. At large energy deposition depths, when $\lambda_{dep} \gg d_0$, the energy of the emitted waves is limited by the destructive interference of the point sources, which also suggests a saturation of A_{xx}, since $E_{SAW} \sim e_{xx}^2 \lambda^2$, and the wavelength of the generated wave is only weakly affected by the energy deposition depth. Importantly, the level of the strain amplitude saturation is above 6×10^{-4}, demonstrating that the laser-induced SAW pulses generated in the thermoelastic regime can be sufficiently strong for the shock front formation and nonlinear coupling to surface processes.

The general character of the observed trends can be illustrated by mapping the conditions of simulations performed with 6 ns pulses (Fig. 7) to those discussed above for 10 ps pulses (Fig. 6). In the simulations performed with 10 ps pulses, the maximum strain amplitude is $\sim 4.6 \times 10^{-4}$, and the effective heat deposition depth, largely defined by the heat diffusion, is $\lambda_{dep} \approx 0.8 d_0$. For a longer 6 ns laser pulse and 32 μm laser spot, $\lambda_{dep} \approx 0.8 d_0$ gives the maximum SAW strain of $\sim 3.8 \times 10^{-4}$. The good agreement of the strain amplitudes obtained for comparable laser energy deposition conditions, but more than two orders of magnitude different pulse durations, supports the general character of the scaling laws revealed in the present study. The relatively small quantitative difference between the two values of A_{xx} may be attributed to the difference in temperature distributions, which are mainly produced by the heat diffusion in simulations illustrated in Fig. 6 and are defined by the Beer–Lambert optical absorption law in the simulations illustrated in Fig. 7.

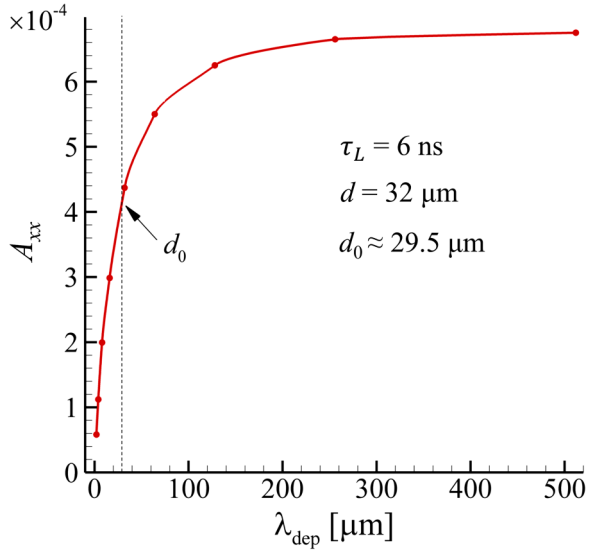

FIG. 7. The dependence of the amplitude of a SAW pulse on the characteristic depth of laser energy deposition. The SAW pulses are generated by 6 ns laser pulses with a flat-top beam profile in the *x*-direction and the laser spot size of $d = 32$ μm. The wave propagation distance during the laser pulse is $d_0 \approx 29.5$ μm.

IV. CONCLUSIONS

The results of the computational analysis of the generation of SAW pulses in a Si substrate irradiated by short laser pulses reveal the general scaling laws describing the dependence of the amplitude and energy of the SAW pulses on the width of the laser beam and suggest the following guidelines for the optimization of the irradiation parameters (pulse duration, spot size, and absorption depth) aimed at the generation of strong SAWs in the thermoelastic regime:

(1) The maximum amplitude of a laser-generated SAW pulse can be achieved when the laser spot size d is comparable to the characteristic length of SAW propagation during the laser irradiation d_0, i.e., $d \approx d_0 = v_{SAW} \tau_L$, where τ_L is the laser pulse duration and v_{SAW} is the speed of the SAW. For spot sizes smaller than the optimum value, the SAW pulse amplitude exhibits a close-to-linear decrease with decreasing d, while for larger spot sizes, the decrease in the wave amplitude follows the $A_{xx} \sim (d + d_0)^{-1}$ scaling.
(2) The amplitude of SAW pulses increases with the increase in characteristic laser energy deposition depth λ_{dep} and saturates at $\lambda_{dep} \sim 2 - 4\, d_0$. Moreover, at $\lambda_{dep} > d_0$, the optimal laser spot size for the maximum strength of the SAW pulses shifts to the values somewhat higher than d_0.
(3) The laser pulses with sharp spatial energy deposition profiles (flat-top laser beams) produce stronger SAWs, and the effect of the beam profile is more pronounced when the depth of the laser energy deposition is large.

At the quantitative level, the results of the simulations demonstrate the ability of nonablative short pulse laser irradiation to generate SAWs with strain amplitudes that are sufficiently high for causing the nonlinear sharpening and shock front formation during the wave propagation in the substrate. In particular, the optimization of irradiation conditions (pulse duration, laser spot size, absorption depth, and the shape of the laser beam profile) can lead to the thermoelastic generation of SAW pulses in a Si substrate with strain amplitudes at the level of 10^{-4}–10^{-3}. The computational predictions support the interpretation of experimental observations of the acoustic activation of surface processes in terms of the dynamic coupling of high-frequency SAW harmonics generated during the nonlinear propagation of SAWs to surface species. More generally, the feasibility of a continuous generation of strong nonlinear acoustic pulses in the thermoelastic regime encourages the exploration of the utilization of acoustic energy for driving various surface

processes in thin film deposition, growth of two-dimensional materials, heterogeneous catalysis, and other applications.

ACKNOWLEDGMENTS

Financial support for this work was provided by the National Science Foundation (NSF) through Grant No. CMMI-1562929. Computational support was provided by the NSF through the Extreme Science and Engineering Discovery Environment (Project No. TGDMR110090) and by Research Computing at the University of Virginia.

AUTHOR DECLARATIONS

Conflict of Interest

The authors have no conflicts to disclose.

DATA AVAILABILITY

The data that support the findings of this study are available from the corresponding author upon reasonable request.

REFERENCES

[1]A. Lomonosov, A. P. Mayer, and P. Hess, "Laser-based surface acoustic waves in materials science, in modern acoustical techniques for the measurement of mechanical properties," in *Experimental Methods in the Physical Sciences*, edited by M. Levy, H. Bass, and R. Stern (Academic Press, San Diego, CA, 2001), Vol. 39, pp. 65–134.
[2]P. Hess, "Surface acoustic waves in materials science," Phys. Today **55** (3), 42–47 (2002).
[3]S. Choi and K.-Y. Jhang, "Internal defect detection using laser-generated longitudinal waves," J. Mech. Sci. Technol. **32**, 4191–4200 (2018).
[4]C. A. Dennett, K. P. So, A. Kushima, D. L. Buller, K. Hattar, and M. P. Short, "Detecting self-ion irradiation-induced void swelling in pure copper using transient grating spectroscopy," Acta Mater. **145**, 496–503 (2018).
[5]F. Hofmann, M. P. Short, and C. A. Dennett, "Transient grating spectroscopy: An ultrarapid, nondestructive materials evaluation technique," MRS Bull. **44**, 392–402 (2019).
[6]L. V. Zhigilei and H. Helvajian, "Acoustic processes in materials," MRS Bull. **44**, 345–349 (2019).
[7]B. Lindner and U. Seydel, "Laser desorption mass spectrometry of nonvolatiles under shock wave conditions," Anal. Chem. **57**, 895–899 (1985).
[8]V. V. Golovlev, S. L. Allman, W. R. Garrett, N. I. Taranenko, and C. H. Chen, "Laser-induced acoustic desorption," Int. J. Mass Spectrom. Ion Processes **169-170**, 69–78 (1997).
[9]J. Pérez, L. E. Ramírez-Arizmendi, C. J. Petzold, L. P. Guler, E. D. Nelson, and H. I. Kenttämaa, "Laser-induced acoustic desorption/chemical ionization in Fourier-transform ion cyclotron resonance mass spectrometry," Int. J. Mass Spectrom. **198**, 173–188 (2000).
[10]A. V. Zinovev, I. V. Veryovkin, J. F. Moore, and M. J. Pellin, "Laser-driven acoustic desorption of organic molecules from back-irradiated solid foils," Anal. Chem. **79**, 8232–8241 (2007).
[11]S. Ehlert, A. Walte, and R. Zimmermann, "Ambient pressure laser desorption and laser-induced acoustic desorption ion mobility spectrometry detection of explosives," Anal. Chem. **85**, 11047–11053 (2013).
[12]K. Benham, F. M. Fernández, and T. M. Orlando, "Sweep jet collection laser-induced acoustic desorption atmospheric pressure photoionization for lipid analysis applications," J. Am. Soc. Mass Spectrom. **30**, 647–658 (2019).
[13]X. Ma, Y. Zhang, H.-R. Lei, and H. I. Kenttämaa, "Laser-induced acoustic desorption," MRS Bull. **44**, 372–381 (2019).
[14]A. A. Kolomenskii, H. A. Schuessler, V. G. Mikhalevich, and A. A. Maznev, "Interaction of laser-generated surface acoustic pulses with fine particles: Surface cleaning and adhesion studies," J. Appl. Phys. **84**, 2404–2410 (1998).
[15]S. Arif, O. Armbruster, and W. Kautek, "Pulse laser particulate separation from polycarbonate: Surface acoustic wave and thermomechanical mechanisms," Appl. Phys. A **111**, 539–548 (2013).
[16]A. M. Lomonosov and P. Hess, "Impulsive fracture of silicon by elastic surface pulses with shocks," Phys. Rev. Lett. **89**, 095501 (2002).
[17]V. V. Kozhushko, A. M. Lomonosov, and P. Hess, "Intrinsic strength of silicon crystals in pure- and combined-mode fracture without precrack," Phys. Rev. Lett. **98**, 195505 (2007).
[18]G. Lehmann, A. M. Lomonosov, P. Hess, and P. Gumbsch, "Impulsive fracture of fused quartz and silicon crystals by nonlinear surface acoustic waves," J. Appl. Phys. **94**, 2907–2914 (2003).
[19]J. K. Wuenschell and H. Helvajian, "Enhanced laser crystallization of thin film amorphous molybdenum disulfide (MoS_2) by means of pulsed laser ultrasound," Opt. Express **27**, 5859–5873 (2019).
[20]A. J. Manzo and H. Helvajian, "Demonstration of enhanced surface mobility of adsorbate cluster species by surface acoustic wave excitation induced by a pulsed laser," Proc. SPIE **8969**, 896908 (2014).
[21]M. V. Shugaev, A. J. Manzo, C. Wu, V. Y. Zaitsev, H. Helvajian, and L. V. Zhigilei, "Strong enhancement of surface diffusion by nonlinear surface acoustic waves," Phys. Rev. B **91**, 235450 (2015).
[22]O. V. Rudenko and S. I. Soluyan, *Theoretical Foundations of Nonlinear Acoustics* (Plenum Publishing Corporation, New York, 1977).
[23]L. K. Naugolnykh and L. Ostrovsky, *Nonlinear Wave Processes in Acoustics* (Cambridge University Press, Cambridge, 1998).
[24]M. V. Shugaev and L. V. Zhigilei, "Mechanisms of acoustic desorption of atomic clusters and exfoliation of graphene multilayers," J. Phys. Chem. C **125**, 23313–23326 (2021).
[25]E. A. Zabolotskaya, "Nonlinear propagation of plane and circular Rayleigh waves in isotropic solids," J. Acoust. Soc. Am. **91**, 2569–2575 (1992).
[26]A. Lomonosov, V. G. Mikhalevich, P. Hess, E. Y. Knight, M. F. Hamilton, and E. A. Zabolotskaya, "Laser-generated nonlinear Rayleigh waves with shocks," J. Acoust. Soc. Am. **105**, 2093–2096 (1999).
[27]M. V. Shugaev, C. Wu, V. Y. Zaitsev, and L. V. Zhigilei, "Molecular dynamics modeling of nonlinear propagation of surface acoustic waves," J. Appl. Phys. **128**, 045117 (2020).
[28]E. Y. Knight, M. F. Hamilton, Y. A. Il'inskii, and E. A. Zabolotskaya, "On Rayleigh wave nonlinearity, and analytical approximation of the shock formation distance," J. Acoust. Soc. Am. **102**, 2529–2535 (1997).
[29]A. A. Kolomenskii, V. A. Lioubimov, S. N. Jerebtsov, and H. A. Schuessler, "Nonlinear surface acoustic wave pulses in solids: Laser excitation, propagation, interactions (invited)," Rev. Sci. Instrum. **74**, 448–452 (2003).
[30]A. A. Kolomenskii and P. Hess, "UV laser excitation of broadband surface acoustic wave pulses in silicon near the ablation threshold," in *Proceedings of IEEE Ultrasonics Symposium* (IEEE, 1994), pp. 651–654.
[31]C. Wu, V. Y. Zaitsev, and L. V. Zhigilei, "Acoustic enhancement of surface diffusion," J. Phys. Chem. C **117**, 9252–9258 (2013).
[32]C. Wu, V. Y. Zaitsev, and L. V. Zhigilei, "Mechanism of acoustically induced diffusional structuring of surface adatoms," Appl. Phys. Lett. **103**, 221601 (2013).
[33]B. S. Yilbas, "Short-pulse laser heating of gold-chromium layers: Thermo-elasto-plastic analysis," J. Phys. D **35**, 1210–1217 (2002).
[34]Y. P. Meshcheryakov and N. M. Bulgakova, "Thermoelastic modeling of microbump and nanojet formation on nanosize gold films under femtosecond laser irradiation," Appl. Phys. A **82**, 363–368 (2005).
[35]D. Y. Tzou and E. J. Pfautsch, "Ultrafast heating and thermomechanical coupling induced by femtosecond lasers," J. Eng. Math. **61**, 231–247 (2008).
[36]Y.-M. Lee and T.-W. Tsai, "Effect of interfacial contact conductance on thermo-elastic response in a two-layered material heated by ultra-fast pulse-laser," J. Phys. D **41**, 045308 (2008).
[37]M. V. Shugaev and N. M. Bulgakova, "Thermodynamic and stress analysis of laser-induced forward transfer of metals," Appl. Phys. A **101**, 103–109 (2010).

[38]M. V. Shugaev, M. He, S. A. Lizunov, Y. Levy, T. J. Y. Derrien, V. P. Zhukov, N. M. Bulgakova, and L. V. Zhigilei, "Insights into laser-materials interaction through modeling on atomic and macroscopic scales," in *Advances in the Application of Lasers in Materials Science*, edited by P. M. Ossi (Springer International Publishing, Cham, 2018), pp. 107–148.
[39]A. J. Manzo and H. Helvajian, "Application of a laser heterodyne technique to characterize surface acoustic waves generated via a pulsed laser excitation," Proc. SPIE **8967**, 89670N (2014).
[40]V. Gusev, A. A. Kolomenskii, and P. Hess, "Effect of melting on the excitation of surface acoustic wave pulses by UV nanosecond laser pulses in silicon," Appl. Phys. A **61**, 285–298 (1995).
[41]D. R. Lide, *CRC Handbook of Chemistry and Physics*, 85th ed. (CRC Press, Boca Raton, FL, 2004).
[42]R. Stoneley, "The propagation of surface elastic waves in a cubic crystal," Proc. R. Soc. London Ser. A **232**, 447–458 (1955).
[43]H. Coufal, K. Meyer, R. K. Grygier, P. Hess, and A. Neubrand, "Precision measurement of the surface acoustic wave velocity on silicon single crystals using optical excitation and detection," J. Acoust. Soc. Am. **95**, 1158–1160 (1994).
[44]A. Tarasenko, R. Čtvrtlík, and R. Kudělka, "Theoretical and experimental revision of surface acoustic waves on the (100) plane of silicon," Sci. Rep. **11**, 2845 (2021).
[45]P. D. Desai, "Thermodynamic properties of iron and silicon," J. Phys. Chem. Ref. Data **15**, 967–983 (1986).
[46]Y. Okada and Y. Tokumaru, "Precise determination of lattice parameter and thermal expansion coefficient of silicon between 300 and 1500 K," J. Appl. Phys. **56**, 314–320 (1984).
[47]J. E. Vidale and R. W. Clayton, "A stable free-surface boundary condition for two-dimensional elastic finite-difference wave simulation," Geophysics **51**, 2247–2249 (1986).
[48]E. D. Palik, *Handbook of Optical Constants of Solids* (Academic Press, San Diego, 1998).
[49]M. V. Shugaev, M. He, Y. Levy, A. Mazzi, A. Miotello, N. M. Bulgakova, and L. V. Zhigilei, "Laser-induced thermal processes: Heat transfer, generation of stresses, melting and solidification, vaporization and phase explosion," in *Handbook of Laser Micro- and Nano-Engineering*, edited by K. Sugioka (Springer, Cham, 2020).
[50]R. W. Ohse and H. von Tippelskirch, "The critical constants of the elements and of some refractory materials with high critical temperatures," High Temp. High Press. **9**, 367–385 (1977).
[51]A. M. Lomonosov, V. V. Kozhushko, and P. Hess, "Laser-based nonlinear surface acoustic waves: From solitary to bond-breaking shock waves," AIP Conf. Proc. **1022**, 481–490 (2008).
[52]G. F. Miller and H. Pursey, "On the partition of energy between elastic waves in a semi-infinite solid," Proc. R. Soc. A **233**, 55–69 (1955).
[53]W. Arnold, B. Betz, and B. Hoffmann, "Efficient generation of surface acoustic waves by thermoelasticity," Appl. Phys. Lett. **47**, 672–674 (1985).
[54]H. M. van Driel, "Kinetics of high-density plasmas generated in Si by 1.06- and 0.53-μm picosecond laser pulses," Phys. Rev. B **35**, 8166–8176 (1987).
[55]T. J.-Y. Derrien and N. M. Bulgakova, "Modeling of silicon in femtosecond laser-induced modification regimes: accounting for ambipolar diffusion," Proc. SPIE **10228**, 102280E (2017).
[56]V. P. Lipp, B. Rethfeld, M. E. Garcia, and D. S. Ivanov, "Atomistic-continuum modeling of short laser pulse melting of Si targets," Phys. Rev. B **90**, 245306 (2014).
[57]G. Paltauf and P. E. Dyer, "Photomechanical processes and effects in ablation," Chem. Rev. **103**, 487–518 (2003).
[58]E. Betzig and J. K. Trautman, "Near-field optics: Microscopy, spectroscopy, and surface modification beyond the diffraction limit," Science **257**, 189–195 (1992).
[59]D. Hwang, S.-G. Ryu, N. Misra, H. Jeon, and C. P. Grigoropoulos, "Nanoscale laser processing and diagnostics," Appl. Phys. A **96**, 289–306 (2009).
[60]I. Falcón Casas and W. Kautek, "Subwavelength nanostructuring of gold films by apertureless scanning probe lithography assisted by a femtosecond fiber laser oscillator," Nanomaterials **8**, 536 (2018).
[61]M. A. Green, "Self-consistent optical parameters of intrinsic silicon at 300 K including temperature coefficients," Sol. Energy Mater. Sol. Cells **92**, 1305–1310 (2008).